Designing optical elements from isotropic materials by using transformation optics

Martin Schmiele, Vineeth S. Varma, Carsten Rockstuhl, and Falk Lederer
Institute of Solid State Theory and Optics, Friedrich-Schiller-Universität Jena, Max-Wien-Platz 1, D-07743 Jena, Germany
(Received 13 December 2009; published 22 March 2010)

By taking advantage of a conformal mapping technique, we propose designs for various optical elements such as directional antennas, flat lenses, or bends. In contrast to most of the existing design approaches, the elements can be implemented with isotropic materials, thus strongly facilitating their fabrication. We furthermore generalize the concept and show that under certain conditions previously suggested devices consisting of anisotropic materials may be replaced by isotropic ones using an appropriate transformation. The designs are double-checked by full-wave simulations. A comparison with their anisotropic counterparts reveals a similar performance.

DOI: 10.1103/PhysRevA.81.033837 PACS number(s): 42.25.Fx, 42.25.Gy, 41.20.Jb

I. INTRODUCTION

The reinterpretation of the form invariance of Maxwell's equations against coordinate transformations by Pendry *et al.* [1] gave birth to the promising field of *transformation optics*. It mainly derives its fascination from the potential to control the mold of light at will and to open doors for applications which contradict our general perception of light propagation. A striking example is illusion optics where an appropriate device may generate the illusion such that an arbitrary object appears to be like some other object of choice [2]. Another example, and historically the first one, is the optical cloak, which is designed to conceal an object from an external observer.

The design of the respective elements exploits that a spatial transformation leads only to transformed material properties as permittivity and permeability. Once the design for a transformational optical device is analytically found, its functionality can be verified using full-wave electromagnetic simulations [3]. For their practical implementation in most cases one relies on metamaterials being artificially nanostructured media allowing one to control the dispersive properties of a propagating wave field [4]. However, in most cases, the anisotropic character of permittivity $\hat{\varepsilon}$ and permeability $\hat{\mu}$ is disadvantageous because it is difficult to implement it by using identical metamaterial unit cells [5]. Consequently, one often resorts to simplified material parameters which will cause a finite scattering [6,7].

Simultaneously with the publication of Pendry *et al.* [1], Leonhardt [8] introduced the concept of *optical conformal mapping*. It can be regarded as a special case of Pendry's concept which only requires a continuous coordinate transformation. In contrast, Leonhardt's concept takes advantage of conformal maps that allow the design of transformation optical devices consisting of isotropic dielectric media. On the other hand, when compared to continuous transformations the mathematical requirements for conformal maps are much more severe. Furthermore, most conformal maps are limited to two-dimensional arrangements. For these reasons most of the designs of transformation optical devices relied on Pendry's concept and thus on anisotropic metamaterials characterized by effective tensors $\hat{\varepsilon}$ and $\hat{\mu}$. Such materials are still hard to realize and concepts that lift this limitation are looked for.

This is mainly driven by the desire to obtain transformation optical devices consisting of more realistic and already available materials. Therefore, an increasing share of research has been devoted to two-dimensional conformal and numerically generated quasi-conformal maps that provide an easier to realize isotropic transformation medium [9]. Li and Pendry designed a ground-plane cloak by a numerical conformal grid generation [10]. Later on this design was realized with nonresonant metamaterial elements in the microwave regime [11] as well as with isotropic dielectric materials in the infrared range [12]. Both designs exhibited only low losses.

However, for a large variety of other devices that are based on transformation optics such isotropic implementations are not yet known. An example is a directional antenna that converts cylindrical waves into plane waves. Such four- and six-beam directional antennas have been studied in Refs. [13–15]. Another example would be a beam bend. Transformation optical structures for beam bends have been discussed in Refs. [16–18]. However, again all of them rely on anisotropic media with different levels of difficulty for a practical realization.

Here we lift this restriction and present design strategies for such antennas relying on conformal Schwartz-Christoffel maps that remedy this disadvantage. However, we admit that this is not the first step toward isotropic devices. Transformation optics waveguides based on isotropic materials have been also studied with the help of numerically generated quasi-conformal maps [19]. Our designs do not allow such flexibility as it can be achieved by numerical methods but do provide easy analytical solutions for the required refractive index distribution.

The manuscript is structured as follows. Section II provides a concise overview on directional antennas in the context of transformation optics. It furthermore briefly reviews the concept of *finite embedded coordinate transformations*. After this we present and discuss our design relying on the conformal mapping technique. In Sec. III we use the results from the previous section in order to design special flat lenses and discuss them in comparison to their anisotropic counterparts as documented in the literature. Most of the extensive calculations used in Secs. II and III may be found in the Appendix. Section IV covers the issue of the beam bend and is divided into three subsections. In Sec. IV A we start with a short review of a known transformation for a beam bend. After this we elaborate a concept that states how and under which conditions an anisotropic material may be replaced by an isotropic one. It is shown that this concept is applicable for the

beam bend. Then we provide full-wave simulations in order to verify the results. Furthermore we also discuss the applicability of the concept to other known transformations. In Sec. IV B we propose a potential practical realization of such an isotropic beam bend where the required pemittivity distribution is mimicked by an effective medium of densely packed dielectric nanocylinders variable in diameter and much smaller than the used wavelength. Such kinds of implementation would be in principle applicable for all the designs we have in mind and shall serve for demonstration purposes. In Sec. IV C we present an alternative and genuine isotropic realization of a right-angle beam bend and compare it to the one from Sec. IV A.

II. DIRECTIONAL ANTENNAS

Directional antennas were investigated in terms of transformation optics in several articles [13–15]. Jiang *et al.* [13,14] used for their designs *finite embedded coordinate transformations* (FECTs), a concept that has been elaborated in the work of Rahm *et al.* [20]. In general such transformations result in anisotropic effective materials $\hat{\varepsilon}$ and $\hat{\mu}$. Furthermore, compared with continuous coordinate transformations, FECTs possess the drawback that reflections may occur at the interface between the outer space and the transformation medium. A criterion for a reflectionless FECT was heuristically found in the initial work on FECTs by Rahm *et al.* [20]. It states that a FECT is reflectionless if the metric in and the metric normal to the interface between the transformation medium and the outer space is continuous. Later on Yan *et al.* [21] presented a thorough investigation on this subject. They found as a necessary and sufficient condition that a FECT is reflectionless if the transformed interface can be represented by a combination of a rotation and a translation of the original interface. Furthermore it turned out that the metric criterion heuristically found in Ref. [20] is too stringent, because only the metric components at the interface must be continuous. The design of a four-beam directional antenna by Jiang *et al.* [13] relies on a FECT that essentially maps a disk onto a square. From simulations they found minor reflections, which is not surprising because a circle cannot be mapped onto a square by a combination of rotation and translation. Furthermore Jiang *et al.* [14] proposed a design for a six-beam lens antenna. They used a continuous as well as a discrete FECT that widens a stripe to a trapezoidal domain. For the discrete FECT the domains were divided into layers. Finally six such trapezoidal antennas were arranged in a hexagon, which transformed a point source into six directed beams. The design with the continuous FECT requires inhomogeneous anisotropic metamaterials whereas the discrete design requires only layers of homogeneous and uniaxial anisotropic metamaterials. Furthermore using the concept of simplified material parameters [3], Jiang *et al.* [14] showed that in contrast to the continuous design the discrete one can even be made reflectionless. Again one can argue that the widening of the stripes to trapezes, which results in a stretching of a line on the interface, cannot be represented by a combined rotation and translation.

In the following we propose directional beam antennas designed by conformal mapping. In contrast to the designs discussed previously they are already realizable with an isotropic medium, which further simplifies possible practical realizations. For the transformation we use *Schwartz-Christoffel transformations* (SCTs). SCTs are conformal maps, which map two-dimensional polygons onto the unit disk or the upper complex half plane. For a brief introduction to SCTs and references for further reading, see Appendix A. First we start with a design for a four-beam directional antenna relying on a SCT from a unit disk onto a square. After that we generalize the design to N-beam directional antennas ($N \geqslant 3$) and discuss the case for $N = 6$, that is, a six-beam directional antenna. The calculations for both designs can be found in Appendices B and C, respectively.

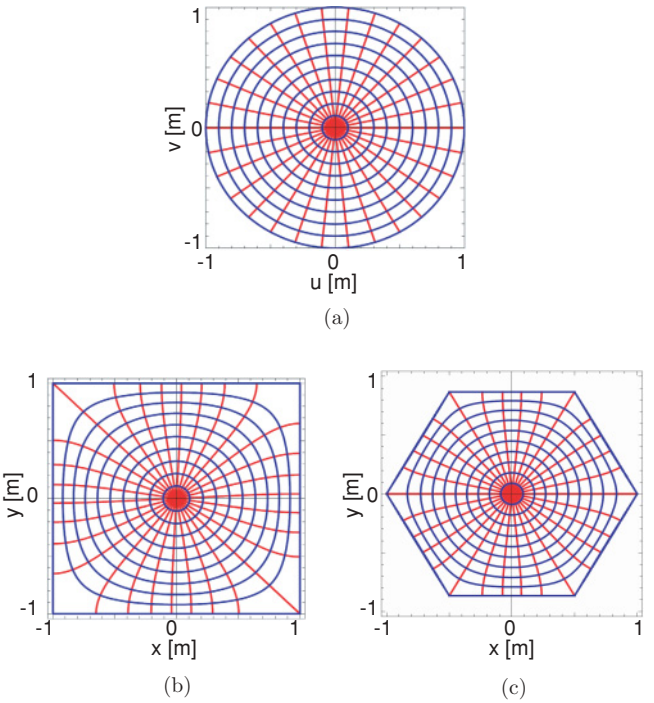

FIG. 1. (Color online) Conformal transformation of a radial and an azimuthal grid in a unit disk in (a) onto a square in (b) and a hexagon in (c). It can be easily deduced that the transformed radial and azimuthal grid lines remain perpendicular to each other.

For the four-beam directional antenna we start with a survey of the properties of the SCT from a unit disk onto a square as derived in Appendix B. There Eq. (B1) together with Eqs. (B2) and (B5) describes the transformation from the unit disk with coordinates $w = u + iv$ onto the square with coordinates $z = x + iy$. Applying the transformation on a grid of constant radial and azimuthal coordinates within a unit disk, as shown in Fig. 1(a), yields a grid inside the square as in Fig. 1(b). The conformal character of the transformation is clearly visible, the grid lines of the constant radial coordinates $|w|$ and azimuthal coordinate $\arg(w)$ remain perpendicular after transformation. The refractive index distribution of this transformation is given in z coordinates by Eq. (B6) together with Eq. (B3) and is depicted in Fig. 2(a). The transformation becomes singular at the four corners of the square. Thus the refractive index approaches 0 there.

In order to obtain a four-beam directional antenna with this transformation a point source must be placed at the origin. In the untransformed w space this would result in a cylindrical wave. In the transformed z space the transformation

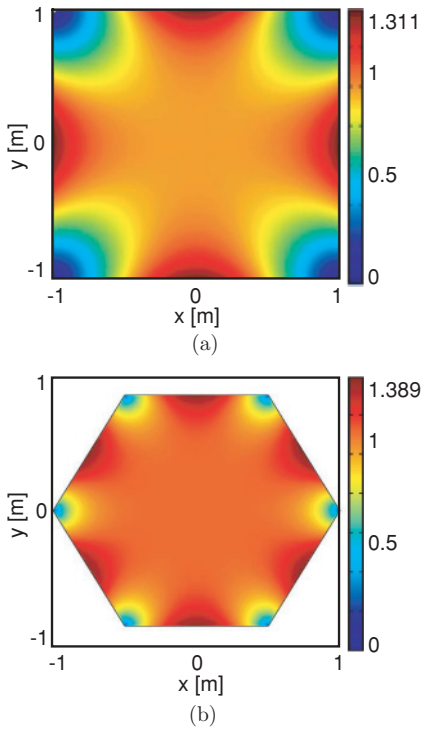

FIG. 2. (Color online) Refractive index distribution according to the transformations from the unit disk onto the square (a) and the hexagon (b). The refractive index approaches 0 at the corners due to the singular behavior of the conformal maps there.

medium transforms this cylindrical wave continuously into four directed beams with a predominantly plane phase front. At the interface with the outer untransformed free space where the square is embedded, the square-shaped wave fronts can cross without refraction due to the fact that they are parallel with the interface. However, due to impedance mismatch with the outer space, reflections do occur. The reflection coefficient R can be estimated by using Fresnel's law for normal incidence

$$R = \left(\frac{n' - 1}{n' + 1}\right)^2, \tag{1}$$

where n' assumes all values $0 \leqslant n' \leqslant 1.311$ at the edge of the square. Over a wide range of segments of the square, R is less than 0.1 ($0.5 \lessapprox n' \leqslant 1.311$). R tends toward 1 at the four corners where n' vanishes.

To verify the functionality of this four-beam directional antenna we proceed by showing results of full-wave simulations. For this purpose we rely on the finite element method (FEM) using `Comsol Multiphysics`. Since Maxwell's equations are scalable and only dielectric materials will be involved, we perform the simulation in the GHz regime. However, an appropriate scaling translates the design to an arbitrary spectral domain as long as materials are on hand having the respective properties. Since a refractive index close to zero is hard to realize we use more realistic conditions. For this purpose we assume that the antenna is embedded in an isotropic background medium with a refractive index of $n' = 1.5$. Therefore according to Fig. 2(a) the refractive index distribution for the square must be scaled by a factor of 1.5. Furthermore, we restrict the lower limit of the scaled

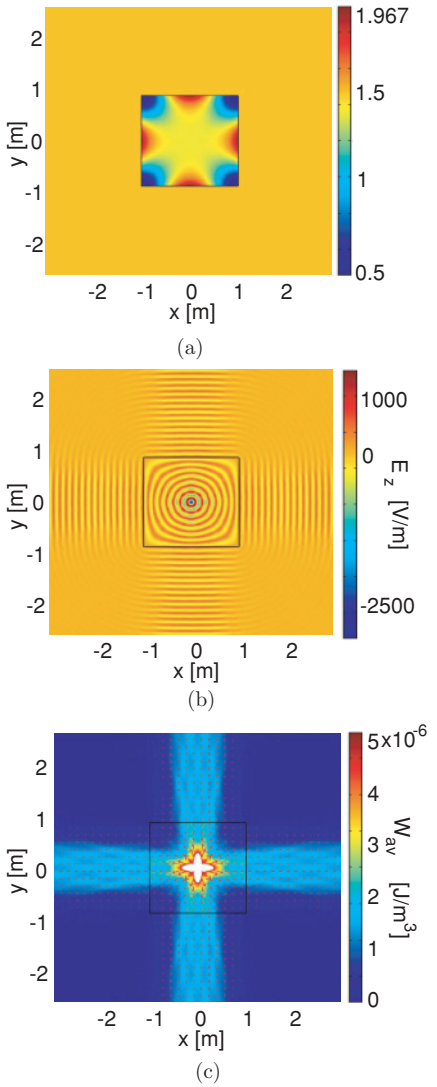

FIG. 3. (Color online) Simulation of the four-beam directional antenna. (a) The refractive index distribution n' that is used and obtained from the one in Fig. 2(a) by scaling with a factor of 1.5 and restricted to $n' > 0.5$. This medium transforms the cylindrical waves emerging from the line source at the origin of panel (b) to quadratic wave fronts that finally form four collimated beams leaving the antenna. Panel (c) shows the corresponding total energy density.

refractive index to $n' = 0.5$. The refractive index distribution obtained by this procedure is depicted in Fig. 3(a). By placing a line source in the origin with an amplitude of $1V/m$ that emits a transverse-electric (TE)-polarized field (electric field perpendicular to the plane of interest) and choosing a free space wavelength of $\lambda = 0.2$ m, the electric field perpendicular to the plane, E_z, and the total energy density, W_{av}, are obtained as shown in Figs. 3(b) and 3(c), respectively. As can be seen, the cylindrical wave fronts emerging from the line source become quadratic with increasing distance. Finally the radiation from the antenna consists of four collimated beams. Only a very minor amount of energy is radiated toward the four corners.

As a generalization from the four-beam antenna to the N-beam antennas, similar SCTs can be found for regular N-gons (see Appendix C) for $N \geqslant 3$. Equation (C2) together

with Eq. (C3) transforms a unit disk (coordinates $w = u + iv$) onto the regular N-gon (coordinates $z = x + iy$). The corresponding refractive index distribution is given by Eq. (C4). For example—and also for a comparison with the design in Ref. [14]—we restrict ourself to the case of a regular hexagon, that is, $N = 6$. The transformation and the corresponding refractive index distribution are depicted in Figs. 1(c) and 2(b), respectively. They show a very similar behavior as in the case of the square. The same simulations as for the square were carried out for the hexagon using directly the refractive index distribution from Eq. (C4) without any scaling and limiting. The results for the electric field perpendicular to the plane and the total energy density are plotted in Figs. 4(a) and 4(b), respectively.

Eventually we briefly compare the isotropic antenna with their anisotropic counterparts from Refs. [13] and [14], respectively. Of course the need for a merely isotropic metamaterial poses a striking simplification for a possible practical realization especially as compared with the design in Ref. [13]. With respect to the problem of impedance mismatch at the outer interface, the design proposed here does not offer any improvements, especially not as compared with the reflectionless design in Ref. [14]. However, the reflection in the isotropic case is very weak and can be theoretically limited to less than 10% over a wide range of beam waists.

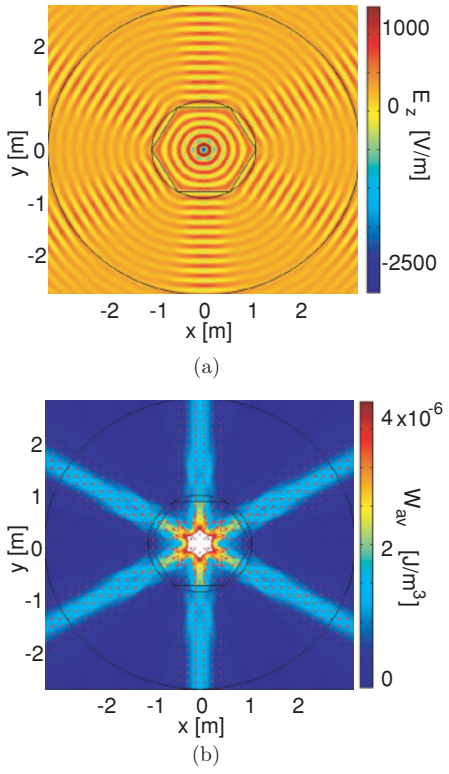

FIG. 4. (Color online) Simulation of an N-beam directional antenna for $N = 6$. Using the refractive index distribution from Fig. 2(b) the cylindrical waves that are emitted from the line source at the origin are transformed to hexagonal wave fronts that finally form the six beams of the antenna. Panel (b) shows the corresponding total energy density.

III. FLAT LENSES

The FECT for a flat lens design from Kwon and Werner [18] transforms a segment of a disk with a plane convex shape to a rectangle. The plane boundary is not modified and is the lower boundary of the rectangle. The convex part of the boundary is mapped onto the upper boundary of the rectangle. Besides the width and the height of the rectangle there is a parameter g that controls the distance of the focus from the lower boundary of the rectangle. One major drawback of this design is again a quite complicated material distribution for the anisotropic $\hat{\varepsilon}$ and $\hat{\mu}$.

Using the concept of simplified material properties as in Ref. [4], one can reduce the problem to nonmagnetic materials. Therefore for transverse magnetic polarization, ε'_{xx}, ε'_{xy}, and ε'_{yy} are multiplied by μ'_{zz} and renamed to $\bar{\varepsilon}'_{ij}$, while $\bar{\mu}'_{zz}$ is set to 1. Maxwell's equations, and therefore the path of the light wave in the lens too, remain unchanged when using the simplified material parameters $\bar{\varepsilon}'_{ij}$ and $\bar{\mu}'_{ij}$. But the intrinsic impedance matching at the lower interface of the lens with the outer space (where the transformation is continuous) is lost. Simulations (not shown here) using a line source at origin for illumination and the simplified material parameters $\bar{\varepsilon}'_{ij}$ and $\bar{\mu}'_{ij}$ show that remarkable reflections occur at the lower boundary of the rectangle, compared with the case of using ε'_{ij} and μ'_{ij}. At the upper boundary of the rectangle there can be principally reflections. This is due to the fact that the transformation is discontinuous there and the criterion for a reflectionless design as given in Ref. [21] is not fulfilled.

Using results of the previous section one can also design a special flat lens exhibiting a major advantage but also a few disadvantages compared with the design described previously. For a four-beam antenna the unit disk was conformally mapped onto a square. Due to the symmetry, the upper half of the unit disk is mapped onto the upper half of the square, that is, a rectangle with a ratio of width to height of 2 : 1. As can be seen from Fig. 3(b), a beam with small divergence impinging on the upper boundary of the square is focused to the origin and would be transformed back to a beam within the lower rectangular part of the square. Hence, if for example only the upper half of the square is used, the plane wave fronts of the beam would be focused onto the origin and from there cylindrical wave fronts would be emitted into the free space in the lower half-plane. The advantage of this design is again an isotropic refractive index distribution (that can be further simplified by the aforementioned scaling and limiting procedure to $n' > n'_{\min} > 0$) compared with the anisotropic one in Ref. [18]. On the other hand several drawbacks emerge from this design compared to the one in Ref. [18]. The most severe one is that the focus is not situated in free space. Instead the focus lies directly on the lower boundary of the flat lens to the outer free space (this corresponds to the case of a focus distance $g = 0$ in the design of Ref. [18]). Another drawback is that reflections may also occur at the lower boundary of the rectangle due to impedance mismatch to the outer free space ($n' \neq 1$ at the boundary). This is a similar problem as already discussed in the case of using simplified anisotropic material properties.

FEM simulations have been carried out to probe this flat lens design. In Fig. 5(a) the flat lens is illuminated by a Gaussian

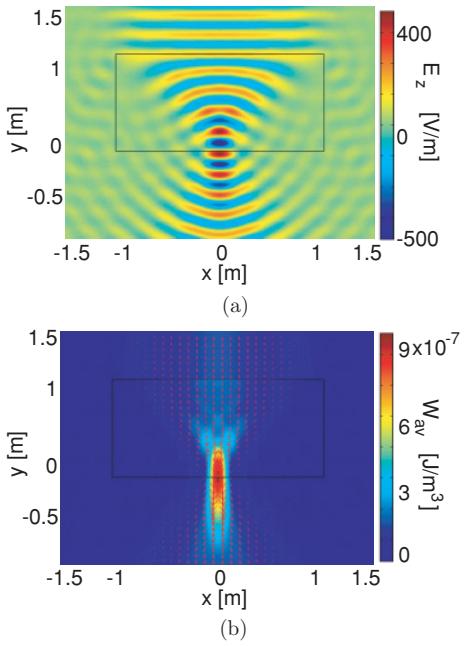

FIG. 5. (Color online) Illumination of the isotropic flat lens from the top by a TE-polarized Gaussian beam with an almost plane phase front. The beam is focused into the origin lying on the lower boundary of the flat lens. From there cylindrical waves emerge and propagate in the lower half-plane. Panels (a) and (b) show the electric field and the corresponding total energy density, respectively.

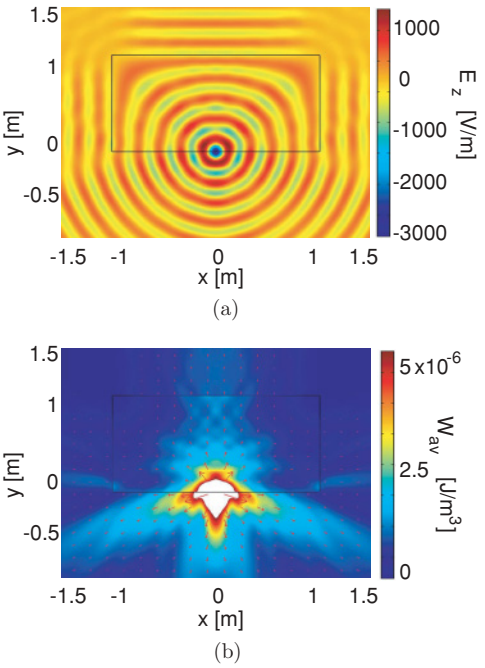

FIG. 6. (Color online) Transformation of a line source placed in the focus of the isotropic flat lens at the bottom edge. The cylindrical waves emitted into the upper half are transformed into plane waves leaving the flat lens via its upper edge but also through its two side edges. The anisotropic flat lens design from Ref. [18] does not suffer from this drawback. Panels (a) and (b) show the electric field perpendicular to the plane and the total energy density, respectively.

beam with an almost plane phase front. Remarkably the beam is focused at the lower boundary of the flat lens and from there cylindrical waves propagate into the lower half plane. Furthermore in Fig. 5(b) the corresponding total energy density and Poynting vectors are plotted. The focusing and defocusing effect are obvious.

While the focusing of a plane wave as in Fig. 5 works properly, the reverse case unveils several drawbacks. In Fig. 6 a line source is placed at the boundary, that is, the focus of the flat lens. For an anisotropic flat lens in Ref. [18] with a focus distance $g = 0$ almost the complete energy that is emitted from the line source into the upper half-space is directed into a beam with a plane phase front, leaving the flat lens through the upper boundary. But using this isotropic flat lens, energy is also transported through the side edges of the rectangle as can be seen from Fig. 6. This is due to the fact that the half circle is mapped onto the upper edge as well as on the two side edges of the rectangle, while in the case of Ref. [18] the half circle is mapped only onto the upper edge of the rectangle. Furthermore from Fig. 6(b) it can be seen that the aforementioned reflections at the lower boundary occur and most of the energy is re-emitted into the lower half-plane. This reduces significantly the efficiency.

Besides the zero focus distance another drawback of this design is that it requires a fixed width to height ratio of 2 : 1. This restriction can be theoretically lifted by computing conformal maps from a rectangle with an arbitrary aspect ratio onto the unit disk (due to symmetry the upper part of such a rectangle is again the image of one half of a unit disk). Such a conformal Schwartz-Christoffel map is already known in the literature (see, e.g., Ref. [22], p. 280, and especially exer. 5 on p. 297) and is briefly derived in Appendix D. The transformation again involves elliptic functions. One issue that could emerge is that even for aspect ratios, R_A, not in excess [for the definition of R_A and its mathematical expression see Appendix D and Eq. (D2)], for example, $R_A = 9$ or $R_A = 10$, the modulus k of the elliptic functions are very close to 1 (deviations in the order of 10^{-12} are found, e.g., for $R_A = 9$ or $R_A = 10$). A similar behavior occurs for small aspect ratios, where the modulus k becomes very close to 0. Hence possibly numerical problems with the evaluation of the elliptical functions should be taken into account when computing the map and its refractive index distribution at very high aspect ratios.

The map from the unit disk with coordinates w onto a rectangle with coordinates z is given by Eq. (D3). Figure 7(a) shows the transformed grid lines of half the unit disk of Fig. 1(a). The corresponding refractive index distribution n' of this transformation is given in z coordinates by Eq. (D5) and is shown in Fig. 7(b) for the same rectangle as in Fig. 7(a). Both graphs are similar to those for the transformation of the square as in Figs. 1(b) and 2(a). As expected the 90° symmetry is reduced to a 180° symmetry.

IV. BENDS

Another example of an optical device for which an isotropic version can be found is beam bends. In Sec. IV A at first we review a known transformation of a beam bend from Ref. [18]. After this we elaborate a concept that allows one to replace the

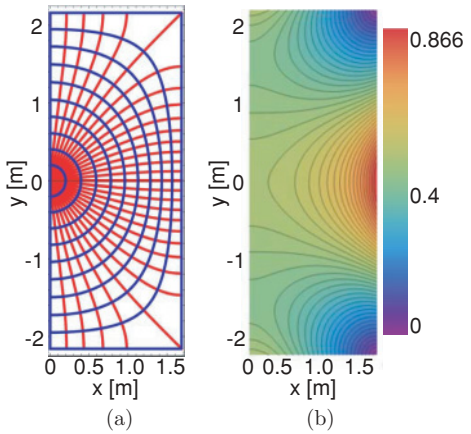

FIG. 7. (Color online) Transformation from the unit disk onto a rectangle. The grid of one half of the unit disk in Fig. 1(a) is transformed by Eq. (D3) to the grid in the half rectangle in panel (a). The corresponding refractive index distribution from Eq. (D5) is shown in panel (b) and shows a form very similar to that of the one for the square in Fig. 2(a).

anisotropic material parameters of this bend by an isotropic medium. After having discussed this isotropic version and the applicability of the concept to other known transformations we proceed in Sec. IV B with a concrete design for this isotropic beam bend based on the effective medium theory for densely packed dielectric nanocylinders. This is exemplarily done as a possible implementation of all the structures we have investigated in this article. Finally, in the Sec. IV C we show an alternative approach to realize an isotropic perpendicular bend. In contrast to the one in Sec. IV A this approach does not rely on the transformation optics concept. We complete the section with a comparison of this beam bender especially to the one from Sec. IV A.

A. Bends made of isotropic media

Kwon *et al.* [18] presented a finite embedded coordinate transformation of a bend that transforms a rectangular grid within a square domain of width w [Fig. 8(a)] into a curved grid [Fig. 8(b)]. For such a perpendicular bend the respective rotation angle amounts to $\beta = \pi/2$. Following the transformation rules from Ref. [18],

$$\rho' = y, \quad \varphi' = \frac{\pi}{2w}(w - x), \quad z' = z, \tag{2}$$

the Jacobian matrix can be computed in primed Cartesian coordinates as

$$\mathcal{J} = \begin{pmatrix} \hat{\mathcal{J}} & 0 \\ & 0 \\ 0\,0 & 1 \end{pmatrix}, \quad \hat{\mathcal{J}} = \begin{pmatrix} \alpha y' & \frac{x'}{\rho'} \\ -\alpha x' & \frac{y'}{\rho'} \end{pmatrix}, \tag{3}$$

where $\rho'^2 = x'^2 + y'^2$ and $\alpha = \beta/w$. To obtain a bend with an isotropic medium later on in this section we use a useful property of this transformation. The transformation is *not conformal* in the x-y plane at all (the Cauchy-Riemann differential equations are not fulfilled or equivalently it holds $\hat{\mathcal{J}}^T/\det\hat{\mathcal{J}} \neq \hat{\mathcal{J}}^{-1}$). This can be also seen from the fact that the vertical lines of constant x in Fig. 8(a) are transformed to radial lines of constant φ' in Fig. 8(b), which are not parallel

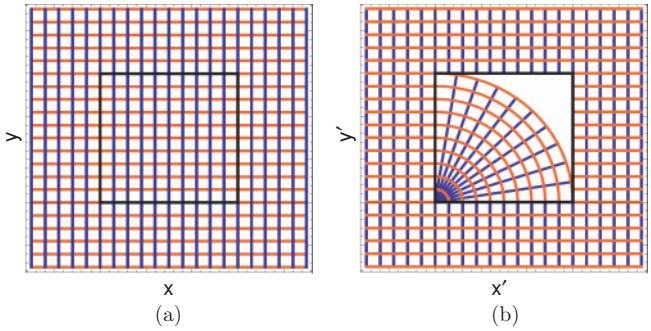

FIG. 8. (Color online) Transformation of the bend from Ref. [18] and used in Sec. IV A for an angle of $\beta = \pi/2$. The Cartesian x-y grid within the quadratic subdomain in panel (a) is transformed in such a way that grid lines of constant y transform into lines of constant radial coordinate ρ' in panel (b) and similarly lines of constant x transform into lines of constant azimuthal coordinate φ'.

anymore. On the other hand for the horizontal lines of constant y in Fig. 8(a), one can see that the transformation shares one characteristic with a conformal map. The lines of constant ρ' remain parallel after transformation and are still perpendicular to the transformed lines of constant x, that is, lines of constant φ'. In the following we refer to these lines of constant y or ρ' as the "*pseudo-conformal directions*" in the bend.

Prior to proceeding with the bend, we present a route of how and under which conditions for the transformation an isotropic medium can be derived from a given anisotropic transformation medium and used as an appropriate alternative. We discuss this procedure with respect to conformal maps and the transformation that possesses a pseudo-conformal direction.

Schurig *et al.* [23] derived a Hamilton formalism for ray tracing in transformation media. The dispersion relation in the anisotropic transformation medium they found is given by

$$\mathcal{H} = \frac{1}{\det\hat{\eta}}[\mathbf{k}'^T\hat{\eta}\mathbf{k}' - \det\hat{\eta}]^2 = 0, \tag{4}$$

with

$$\hat{\eta} = \hat{\varepsilon}' = \hat{\mu}' = \frac{\mathcal{J}\mathcal{J}^T}{\det\mathcal{J}}, \tag{5}$$

where it was assumed that the untransformed space is vacuum, that is, $\hat{\varepsilon} = \hat{\mu} = 1_3$. Furthermore $k_0\mathbf{k}'$ denotes the wave vector in the transformation media where $k_0 = 2\pi/\lambda_0$ with λ_0 as the free space wavelength.

One can show that this formalism is analogously applicable for an inhomogeneous and dispersive but still isotropic distribution of $\varepsilon = \varepsilon(\mathbf{r}, \omega)$ and $\mu = \mu(\mathbf{r}, \omega)$ in the untransformed space. Therefore, one only has to replace $\hat{\eta}$ in Eq. (4) by $\sqrt{\varepsilon\mu}\cdot\hat{\eta}$. With $n(\mathbf{r}, \omega) = \sqrt{\varepsilon\mu}$ as the isotropic, but inhomogeneous refractive index in the untransformed space, one gets

$$\frac{1}{\det(n\cdot\hat{\eta})}[\mathbf{k}'^T(n\cdot\hat{\eta})\mathbf{k}' - \det(n\cdot\hat{\eta})]^2 = 0. \tag{6}$$

Equation (6) can be simplified to

$$\frac{n^2}{\det\mathcal{J}}[(\mathcal{J}^T\mathbf{k}')^2 - n^2]^2 = 0. \tag{7}$$

Assuming that $\mathcal{J}$ is nonsingular and setting $\mathbf{k}' = n' \cdot \bar{\mathbf{k}}'$, where $\bar{\mathbf{k}}'$ is a dimensionless unit vector, the refractive index distribution n' as a function of the transformed coordinates $\mathbf{r}'$ and $\bar{\mathbf{k}}'$ can be written as

$$n'(\mathbf{r}', \bar{\mathbf{k}}') = \|\mathcal{J}^T \bar{\mathbf{k}}'\|^{-1} \cdot n(\mathbf{r}'). \tag{8}$$

Due to the fact that the wave vector $(-\omega/c, \mathbf{k})$ is a four-vector it transforms under coordinate transformations (in space and time) just by applying the 4×4 Jacobian matrix. For purely spatial coordinate transformations, the (spatial part of the) wave vector in the untransformed frame $k_0\mathbf{k}$ transforms to $k_0\mathbf{k}'$ in the transformed frame via $\mathbf{k}' = \mathcal{J}\mathbf{k}$. Therefore, $\bar{\mathbf{k}}'$ is linked with $\mathbf{k}$ via the expression

$$\bar{\mathbf{k}}' = \frac{\mathcal{J}\mathbf{k}}{\|\mathcal{J}\mathbf{k}\|}. \tag{9}$$

The quantity n' in Eq. (8) can be considered as the refractive index that light experiences at a point $\mathbf{r}'$ in the direction of $\bar{\mathbf{k}}'$ inside the anisotropic transformation medium of $\hat{\varepsilon}'$ and $\hat{\mu}'$.

Hence for a desired spatial distribution of propagation directions $\bar{\mathbf{k}}'$ in the transformation medium, one can compute for every point the refractive index n'.

But it is important to state that in general one would not obtain the same light ray trajectories along the desired $\bar{\mathbf{k}}'$ distribution if one would simply replace the anisotropic material by $\hat{\varepsilon}'$ and $\hat{\mu}'$ with the isotropic one of n'.

Two-dimensional conformal maps are an exception. One can show that in this case Eq. (7) reduces to the known result as in Ref. [8] [Eq. (A2)]. For a two-dimensional conformal map $z(w)$ with $z = x + iy$ and $w = u + iv$ it holds that $\hat{\mathcal{J}}^T\hat{\mathcal{J}} = \det\hat{\mathcal{J}}\,1_2 = |dz/dw|^2 1_2$ because of the Cauchy-Riemann differential equations ($u_x = v_y$ and $u_y = -v_x$). For propagation in the untransformed two-dimensional plane with an in-plane wave vector $\mathbf{k} = \mathbf{k}_\parallel$ ($k_z = 0$), Eq. (8) can be written as

$$\begin{aligned} n' &= \left\| \mathcal{J}^T \frac{\mathcal{J}\mathbf{k}_\parallel}{\|\mathcal{J}\mathbf{k}_\parallel\|} \right\|^{-1} \cdot n = \frac{\sqrt{\mathbf{k}_\parallel^T \mathcal{J}^T \mathcal{J}\mathbf{k}_\parallel}}{\|\mathcal{J}^T\mathcal{J}\mathbf{k}_\parallel\|} \cdot n \\ &= \frac{\sqrt{\mathbf{k}_\parallel^T\mathbf{k}_\parallel}}{\|\mathbf{k}_\parallel\|} \cdot \frac{n}{\sqrt{|\det\mathcal{J}|}} = \left|\frac{dz}{dw}\right|^{-1} \cdot n, \end{aligned} \tag{10}$$

which is in accordance with Eq. (A2). Hence for a conformal map it is possible to use the easier isotropic refractive index distribution n' instead of the anisotropic $\hat{\varepsilon}'$ and $\hat{\mu}'$ without changing the ray path in the transformation medium.

However, in particular for the bend this replacement is *only possible along the pseudo-conformal direction* [$\mathbf{k} = (1, 0, 0)^T$ in the untransformed space]. With the bend's Jacobian in Eq. (3) and a light propagation direction of $\mathbf{k} = (k_x, k_y, 0)^T$ in the untransformed free space ($\|\mathbf{k}\| = \sqrt{k_x^2 + k_y^2} = 1$), n' can formally be calculated by Eqs. (8) and (9) as

$$n' = \frac{\sqrt{\alpha^2\rho'^2 k_x^2 + k_y^2}}{\alpha^2\rho'^2 k_x + k_y}. \tag{11}$$

For the pseudo-conformal direction of $\mathbf{k} = (1, 0, 0)^T$ it simplifies to

$$n' = (\alpha\rho')^{-1}. \tag{12}$$

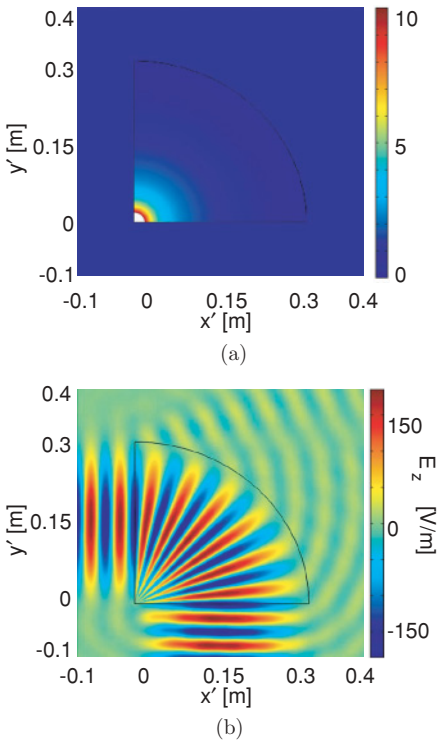

FIG. 9. (Color online) (a) Refractive index distribution for the isotropic perpendicular bend of width $w = 0.3$ m from Eq. (12) in Sec. IV A. For better visual perception, the shown refractive index is limited to $n' = 10$. (b) Propagation of a TE-polarized Gaussian beam at a free space wavelength of $\lambda_0 = 0.05$ m that impinges from the left on the bend.

To double-check the performance of the isotropic bend we again perform full-wave simulations. In Fig. 9(b) a TE-polarized Gaussian beam with a free space wavelength of $\lambda_0 = 0.05$ m impinges on the bend from the left-hand side with a width of $w = 0.3$ m. Most of the electric E_z field in Fig. 9(b) is smoothly perpendicularly bent in a clockwise direction and leaves the bend through the lower interface into free space. Nevertheless one issue that arises when using the isotropic n' instead of the anisotropic material as in Ref. [18] is the impedance mismatch at the interface to the free space. Using the anisotropic medium no reflections occur at the left interface $L' = \{(x', y')|x' = 0, y' \in [0, w]\}$ because there the transformation is continuous and hence the transformation medium is intrinsically impedance matched to the free space. By contrast, at the bottom interface $B' = \{(x', y')|x' \in [0, w], y' = 0\}$ where the transformation is discontinuous with the outer free space, no reflections occur, too. This can be explained by the aforementioned criterion from Ref. [21], because the transformation of the right-hand interface $R = \{(x, y)|x = w, y \in [0, w]\}$ in the original space to B' in the transformed space can be regarded as a combination of a clockwise rotation of 90° degrees and a translation of $-w$ along the x direction.

It is important to note that the functionality of the isotropic beam bender is limited to normal incidence. First, this is due to the fact that n' was calculated under this assumption, and second, only for normal incidence does refraction vanish at L' and B'. This also means that the bend can only be used

for beams with a sufficiently small divergence ($k_y \ll k_x \approx 1$ for the incident beam in our geometry). For the anisotropic bend these limitations do not apply; that is, it works also for obliquely incident and divergent beams.

For a possible practical realization the refractive index distribution as in Eq. (12) is still inappropriate due to its singular behavior for small radii ρ which causes the index to approach zero. This problem can be lifted by introducing upper and optionally also lower limits for n' (the lower limit may not be necessary since n' approaches $2/\pi = 0.637$ at $\rho' = w$). Furthermore w must be adjusted in such a way that the ring segment that is not affected by the limiting procedure fits to the waist of the impinging beam. Figure 10(a) shows the refractive index distribution for a bend with $w = 0.8$ m and the restriction $2 \leqslant n' \leqslant 4$. In Fig. 10(b) this bend is illuminated by a TE-polarized Gaussian beam with a suitable beam waist of 0.16 m and a free space wavelength of 0.05 m. Figure 10(c) shows the corresponding total energy density. It is obvious that for a given beam waist the necessary refractive index range can be adjusted by changing the bend radius, that is, w. The larger w is the smaller the refractive index range is. Reducing the index range and using a refractive index in the outer space that lies in this index region can also be utilized to reduce reflections at the interface to the outer space to acceptable values.

Before we proceed with the next section the applicability of the concept, presented previously for nonconformal maps, is discussed. However, to make it clear from the very beginning, besides the beam bender we did not succeed in finding any other nontrivial transformations among the many ones suggested in the literature, where pseudo-conformal directions do exist and are also relevant for the functionality of the transformation optical device. A trivial example is squeezing a rectangle to half of its width, that is, $x' = x/2$. According to Eqs. (8) and (9) this would require $n' = 2n$ for light propagating into the x direction.

For two-dimensional cylindrical cloaks with transformations of the kind $\rho' = \rho'(\rho)$ and $\theta' = \theta$ the coordinate lines along ρ and θ remain orthogonal after transformation; that is, they are pseudo-conformal directions. But this does not help. To cloak an object that is illuminated by a plane wave (or a beam with low divergence) propagating along the x direction, the pseudo-conformal direction must be the x direction too, in order to use the corresponding isotropic media. But one can easily show that the coordinate lines along the transformed x' and y' directions will never be orthogonal as for the untransformed x-y grid for any function $\rho'(\rho)$. Making use of the chain rule, one obtains the following for the scalar product of the unit vectors along the x' and y' coordinate lines:

$$\begin{aligned}\mathbf{e}_{x'} \cdot \mathbf{e}_{y'} &\sim \frac{\partial \mathbf{r}}{\partial x'} \cdot \frac{\partial \mathbf{r}}{\partial y'} \\ &= \left(\mathbf{e}_\rho \frac{\partial \rho}{\partial \rho'} \frac{x'}{\rho'} - \mathbf{e}_\theta \frac{\rho}{\rho'} \frac{y'}{\rho'}\right) \cdot \left(\mathbf{e}_\rho \frac{\partial \rho}{\partial \rho'} \frac{y'}{\rho'} + \mathbf{e}_\theta \frac{\rho}{\rho'} \frac{x'}{\rho'}\right) \\ &= \frac{x'y'}{\rho'^2}\left[\left(\frac{\partial \rho}{\partial \rho'}\right)^2 - \left(\frac{\rho}{\rho'}\right)^2\right] \stackrel{!}{=} 0.\end{aligned}$$

The condition requiring that the obtained differential equation $\partial\rho/\partial\rho' = \rho/\rho'$ for $\rho'(\rho)$ shall hold together with the boundary condition, that $\rho'(\rho)$ must be continuous at least across the outer boundary of the cloak, gives merely the trivial solution $\rho' = \rho$, that is, the identity transformation. Hence for such types of cloaks no equivalent isotropic alternative can be used.

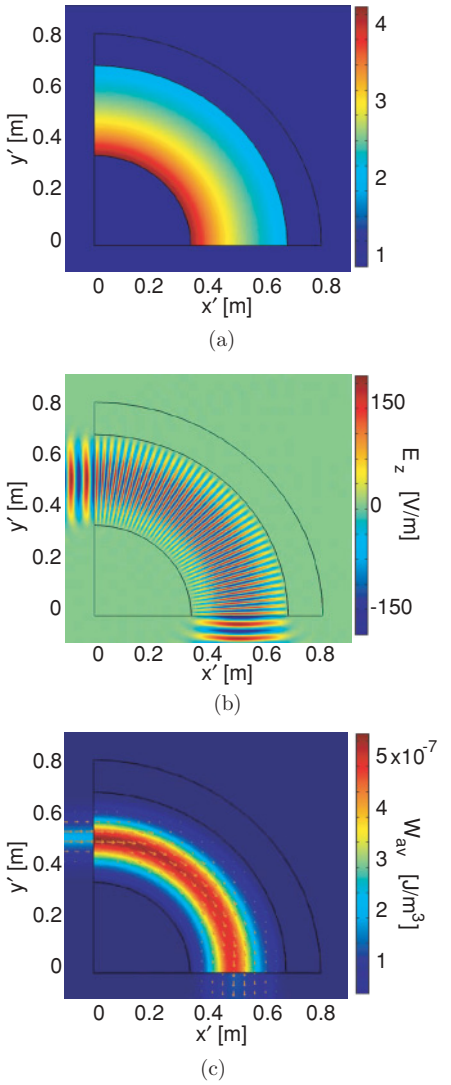

FIG. 10. (Color online) Simplified model of the isotropic bend from Fig. 9. The large refractive index for small radii can be avoided by increasing the bend radius. This can be achieved by increasing w, considerably exceeding the waist of the incoming beam, as well as by ensuring that the beam propagates in a ring segment with a sufficiently large radius. This has been done in Fig. (a) for the bend with $w = 0.8$ m. The ring segment between the radii of 0.318 and 0.637 m provides a refractive index in the range $n' \in [2,4]$. Finally, panels (b) and (c) show the electric field and the total energy density of a TE-polarized Gaussian beam with a beam waist of 0.16 m and a free space wavelength of 0.05 m, respectively, impinging from the left at the center of the ring segment ($y' = 0.477$ m).

Another problem that arises is that even if one has found a usable pseudo-conformal direction, the intrinsic impedance matching at the interface between transformed and untransformed space is not automatically fulfilled if the anisotropic quantities $\hat{\varepsilon}'$ and $\hat{\mu}'$ are replaced by the isotropic n' one. In the bend light enters and leaves it normal to the interfaces, which "only" results in reflections at the interfaces and diminishes

the performance. But in general, theses interface problems can be more severe. For oblique incidence, refraction and total reflection can occur at the interface preventing the use of the isotropic device. These problems do not occur if the transformation is continuously differentiable at the interface, because then n' will be continuous there.

B. Implementation of the bend by using dielectric nanocylinders

To outline a possible bend implementation and to evaluate its performance beyond a description that is based on an effective refractive index we have rigorously simulated such bends where the index distribution is realized by spatially distributed dielectric cylinders of varying size [24].

In particular, we started from the index distribution of a bend as given by Eq. (12), assumed a width of $w = 0.27$ m, and discretized the index profile on a grid where each grid point had a size of a tenth of the wavelength. The design wavelength was again 0.05 m. At each grid point we located a dielectric cylinder whose radius was adjusted to evoke the required effective index. We mention that the size of the cylinder was sufficiently small for the effective medium model to hold. Since the dielectric cylinder is nonresonant in the spectral domain of interest, the effective permittivity can be assigned, in principle, by computing the spatial average of the permittivity in the unit cell. Nevertheless, rigorous simulations were used to verify this assumption [25,26]. For the dielectric material of the cylinder we assumed a semiconductor with $\varepsilon = 13$. The cylinders were surrounded by air. The refractive index distribution was strictly limited to values obtainable within this material system, for example, no index lower than unity or larger than $\approx$3.6 was possible.

The ensemble of cylinders was illuminated by a Gaussian beam (beam width corresponds to the wavelength) whose waist was placed at the entrance facet of the bend. With the above design constraints the bend consisted of 1553 cylinders and the entrance facet had a width of 26 cylinders. For the rigorous simulations a multiple scattering formalism was used [27]. The evolving amplitude distribution for this device can be seen in Fig. 11(a). Nearly all light is bent within the structure. The only loss mechanisms are back reflections at the interface since the impedance is not matched to the outer domain and some light that leaks out of the device since the width of the bend is too small and the wave nature of light does not allow for a perfect confinement.

To access in more detail the properties, the bent, the reflected, and the maximum amount of bent light for negligible reflection are shown in Fig. 11(b) as a function of the bend width. This width was continuously increased and quantified by the number of cylinders that form the entrance facet. Two things can be seen. First, Fabry-Perot oscillations of the light inside the bend cause a sinusoidal modulation of the amount of bent and reflected light. The geometry with 26 cylinders was chosen since it corresponds to a maximum in the bent energy at negligible reflection. Therefore, despite being not impedance matched, reflection may be strongly suppressed. Second, the larger the bend width and the smoother the index profile, the larger the maximum possible bent efficiency which asymptotically converges toward 100%. The smoother the index gradient and the larger the bend when compared

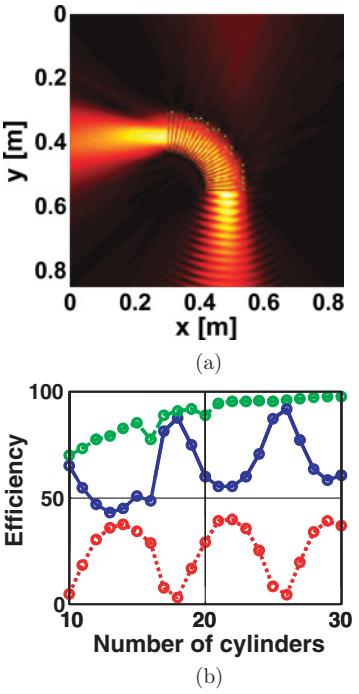

FIG. 11. (Color online) (a) Amplitude distribution upon illuminating a bend consisting of periodically arranged dielectric cylinders of spatially varying radius to cause an effective index according to that shown in Eq. (12) with a width of $w = 0.27$ m. The cylinders are made of a semiconductor with $\varepsilon = 13$ and are embedded in air. The index distribution is limited to those values that can be obtained with this material basis. The structure is illuminated by a Gaussian beam of a width of 0.05 m and which propagates in the negative y direction. For the specific example 26 cylinders form the entrance facet of the bend. The cylinders are indicated by green circles, though they are hardly discernible since their density is large. (b) Share of bent light [blue (black) solid line], reflected light [red (dark gray) dotted], and the maximum attainable bend efficiency [green (light gray) dashed line], shown in percent, as a function of the bend size. The size is quantified by the number of cylinders that form the entrance facet. Lines are only a guide to the eye since the size cannot be adjusted continuously.

to the wavelength, the smaller is the leakage of the light out of the structure and the more light can be efficiently transmitted.

This potentially practical realization of a bend has exemplarily proven that the translation of a device that was designed by transformation optics and where only an isotropic index was required can be obtained with such a simple nanostructured system.

C. An alternative isotropic perpendicular bend

An alternative approach for a two-dimensional beam splitter was derived in terms of an appropriate refractive index distribution already more than 15 years ago [28]. This beam splitter is a disk with a radius R. A collimated beam that symmetrically impinges on the disk's center is symmetrically split such that either outgoing beam leaves the splitter at an angle of $q\pi/2$ $(0 \leqslant q \leqslant 4)$ with respect to the incident beam. Variable beam division can be achieved by displacing

the incident beam transversely with respect to the radial axis pointing to the origin.

Here we use this beam splitter as a bend, which is possible if the beam thickness is less than the disk radius R and the beam is sufficiently transversely displaced that it will not hit the origin anymore. Considering a coordinate system with radial coordinate ρ and the dimensionless variable $r = \rho/R$, the radially symmetrical refractive index distribution $n(r)$ of this beam splitter is determined by

$$r^2(1+\sqrt{1-(rn)^2})^{q-2} = (rn)^q, \tag{13}$$

where q controls the bending angle. This equation for the refractive index distribution was derived in Ref. [28] (see Eq. III.6.12 on p. 599) without using transformation optics methods, which were unknown at that time. For a cylindrically symmetric refractive index distribution $n(r)$ the ray equations can be written as a separable first-order differential equation in r and the azimuthal coordinate. Integration of the r-dependent side leads to an Abelian integral that must be solved (for a more comprehensive description see Chap. 4.7 and Appendix III.6 in Ref. [28]). In order to proceed, after some calculations Eq. (13) for $n(r)$ can be rewritten in the form

$$r^\nu\left(1-\frac{2}{r}n^{\frac{\nu}{2}-1}+n^\nu\right)=0, \tag{14}$$

where $\nu = 4/(2-q)$. For $q = 0$, or equivalently $q = 4$, that is, for a 2π retro reflector, it can be shown that the solution for the refractive index law $n(r)$ in Eq. (14) is that of an Eaton lens [28].

From now on we focus on the bend. The easiest case—and maybe the only one with an analytical solution for $n(r)$—is the one of a perpendicular bend, that is, $q = 1$ ($\nu = 4$) or equivalently $q = 3$ ($\nu = -4$). Either value of ν simplifies Eq. (14) to

$$1-2\frac{n}{r}+n^4=0. \tag{15}$$

Equation (15) provides four solutions for $n(r)$, but only one of them is physically relevant. With the help of a computer-algebra system like `Wolfram Mathematica` a solution for $n(r)$ can be easily derived and can be expressed as

$$\begin{aligned} n(r) &= \frac{\mu(r)}{\sqrt[3]{2}}\left(1+\sqrt{\frac{1}{r\cdot\mu(r)^3}-1}\right),\\ \mu(r) &= \frac{1}{\sqrt[4]{3}\cdot\sqrt[6]{2}}\sqrt{\frac{1}{\Omega(r)}+\Omega(r)},\\ \Omega(r) &= \frac{\sqrt{3}}{\sqrt[3]{4}}r^{-2/3}\left(1+\sqrt{1-\frac{16}{27}r^4}\right)^{1/3}. \end{aligned} \tag{16}$$

This refractive index is plotted in Fig. 12(a). It diverges to $+\infty$ if r approaches 0 and converges toward 1 for $r = 1$, that is, $\rho = R$, so that there is a continuous transition at the interface to the outer domain.

To verify the functionality of this kind of bend, full-wave simulations have been carried out. In Fig. 12(b) a TE-polarized Gaussian beam of the form $E_z = \exp[-(y-y_0)^2/w_0^2]\mathrm{V/m}$ ($y_0 = 0.5$ m, $w_0 = 0.25$ m) with a free space wavelength of

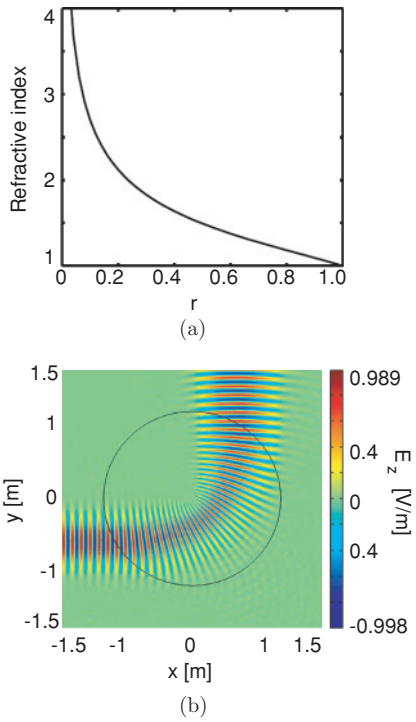

FIG. 12. (Color online) (a) Radial refractive index profile $n(r)$ for the perpendicular bend according to Eq. (16). While the refractive index diverges for small radii $\rho = rR$, it exhibits a continuous transition to the outer space at the interface, that is, for $r = 1$. (b) Propagation of a TE-polarized Gaussian beam through a bend with a radius of $R = 1$ m confirming its functionality.

$\lambda_0 = 0.1$ m impinges at a bend with a radius of $R = 1$ m and experiences a $\pi/2$ turn to the left side.

To conclude on this kind of bend in the following we compare some key parameters with the other bend types. Compared to its anisotropic versions [16–18] it is advantageous with respect to its simpler realization in an isotropic medium. Like the anisotropic devices it is perfectly impedance matched at both ends.

Compared with the other isotropic bends as presented in Sec. IV A, it exhibits a similar though more complicated refractive index distribution. But compared with the numerically computed isotropic bend of Ref. [19] it lacks from a singular behavior of $n(r)$ for small radii, similar to the bend from Sec. IV A. A striking advantage against both other isotropic counterparts is impedance matching.

A general drawback of this bend is its low flexibility with regard to bending angles other than $\pi/2$. Analytical solutions for $n(r)$ from Eq. (14) for bending angles $q\pi/2$ with $q \neq 1, 3$ are not expected to exist. None of the anisotropic bends or the other isotropic bends suffer from this restriction.

V. CONCLUSIONS

To sum up, we significantly reduced the requirements for the transformation medium of directional antennas and flat lenses. Our designs, relying on conformal Schwarz-Christoffel transformations, work already with isotropic dielectric media. Furthermore, if certain conditions regarding the transformation hold, we put forward a concept to replace the anisotropic

material, usually required in transformation optics designs, by an isotropic refractive index distribution where a similar optical behavior can be obtained. We showed that this concept is applicable for a known transformation of a bend and that it provides a simple analytical expression for the refractive index distribution.

In the present work we focused on an analytical approach in the designs. However, for a greater flexibility in the design process of transformation optical devices the use of numerical conformal grid generators like `CONFPACK` [29], `Zipper` [30], or those used in the papers of Li and Pendry [10] and Landy and Padilla [19] are inevitable. With regard to future practical implementations of transformation optical devices it may be anticipated that the use of conformal mapping techniques is a much more promising approach despite their more sophisticated calculation.

ACKNOWLEDGMENTS

This work was partially supported by the German Federal Ministry of Education and Research (MetaMat, PhoNa) and by the Thuringian State Government (MeMa). The work of V. S. Varma was supported by the EU.

APPENDIX A: SCHWARZ-CHRISTOFFEL TRANSFORMATIONS

In this section we provide a concise introduction to conformal Schwarz-Christoffel transformations (SCTs), for a more detailed introduction see, for example, Ref. [22] or other textbooks on conformal mapping. SCTs allow one to map two-dimensional polygons onto the upper complex half-plane or the unit disk (which is conformally equivalent to the half-plane). For a polygon with N vertices the SCT can be written as

$$z(w) = A \int \prod_{k=1}^{N} (w - w_k)^{-(1-\alpha_k/\pi)}\, dw + B. \tag{A1}$$

Here w denotes the coordinates in the upper complex half-plane or in the unit disk and z denotes those in the polygon. The α_k denotes the polygon's interior angles and the $w_k = w(z_k)$ are the images of the polygon's vertices z_k. In the case of mapping to the upper complex half-plane the w_k lie on the real axis whereas for the unit disk they lie on the unit circle $|w| = 1$. A and B are (complex) constants that represent two degrees of freedom for an overall rotation (A) and translation (B) of the map. It can be shown that it is always possible to drop one of the N factors (i.e., one vertex) in the integrand's product series without changing the SCT.

The transformed refractive index distribution n' for a SCT is given like for conformal maps by [8]

$$n' = \left|\frac{dw}{dz}\right| n, \tag{A2}$$

where n is the refractive index distribution in the untransformed space.

In the following three appendices we give the results for the SCTs and their associated refractive index distributions that are used in Secs. II and III. To perform symbolic integrations of the SCT integrals, as in Eq. (A1), the computer-algebra system `Wolfram Mathematica` was used.

APPENDIX B: SCT FROM A SQUARE ONTO THE UPPER COMPLEX HALF-PLANE AND THE UNIT DISK

In this section a SCT from a square (coordinates z) onto the upper half-plane (coordinates q) is derived via Eq. (A1). By another conformal map the upper half-plane is subsequently mapped onto the unit disk (coordinates w). As mentioned in Appendix A only three of the four vertices of a square must be considered. Setting the angles $\alpha_k = \frac{\pi}{2}$, $k = 1, 2, 3$, and choosing the points $q_1 = -1$, $q_2 = 0$, $q_3 = 1$ on the real axis of the upper half-plane, the SCT from a square onto the upper complex half-plane can be written with Eq. (A1) as

$$z(q) = A \int (q^2 - 1)^{-\frac{1}{2}} q^{-\frac{1}{2}} dq + B,$$

which leads after integration to

$$z(q) = A \cdot 2i \cdot F\left(i \sinh^{-1}\left(\frac{1}{\sqrt{q-1}}\right)\middle| 2\right) + B. \tag{B1}$$

Here $F(\varphi|m)$ denotes the incomplete elliptic integral of the first kind with the elliptic modulus m. With the constraints $z(-1) = -1 - i$ and $z(1) = 1 + i$ the square is fixed to an edge length of 2 and in an upright position. Thus the coefficients A and B are obtained as

$$A = -\frac{2 + 2i}{2K(-1) + i\sqrt{2}K\left(\frac{1}{2}\right)}, \qquad B = -1 + i, \tag{B2}$$

where $K(m)$ denotes the complete elliptic integral of the first kind. The inverse transformation of Eq. (B1) is given by

$$q(z) = 1 - \frac{1}{\mathrm{sn}\left(\frac{2i\sqrt{2}\pi^{3/2}[z+(1-i)]}{\Gamma\left(-\frac{1}{4}\right)^2}\middle| 2\right)^2}, \tag{B3}$$

where $\mathrm{sn}(\varphi|m)$ denotes the Jacobi elliptic function (it holds $\mathrm{sn}[F(\varphi|m)|m] = \sin\varphi$) and Γ the Gamma function. Thus the transformed refractive index distribution can be written as a function of z as

$$n'(z) = \left|\frac{dz}{dq}\right|^{-1} n(q) = \left|\frac{[q(z)^2 - 1]^{\frac{1}{2}} q(z)^{\frac{1}{2}}}{A}\right|. \tag{B4}$$

Here and in the following we assume a constant refractive index distribution $n(q) = 1$ in the q or w space. The map from the square onto the unit disk can be obtained comparatively easily. Due to the fact that the upper half-plane and the unit disk (coordinates w) are connected by the invertible conformal map,

$$q(w) = i\frac{1 + w}{1 - w}, \tag{B5}$$

a combination of Eqs. (B1) and (B5) gives the desired transformation between the square and the unit disk. The refractive index distribution of this combined transformation is obtained by using the chain rule and can be written in the square's z coordinates as

$$n'(z) = \left|\frac{dz}{dq}\frac{dq}{dw}\right|^{-1} = \left|\frac{2[q(z)^2 - 1]^{\frac{1}{2}} q(z)^{\frac{1}{2}}}{A\,[i + q(z)]^2}\right|. \tag{B6}$$

Thereby the coordinates w in the expression for dq/dw have been replaced by the coordinates $q = q(z)$ using the inverse of Eq. (B5).

APPENDIX C: SCT FROM A REGULAR N-GON ONTO THE UNIT DISK

It can be shown (see, for example, exer. 4 on p. 196 in Ref. [22]) that the transformation

$$z(w) = A \int (1 - w^N)^{-2/N} dw + B \tag{C1}$$

maps a regular N-gon (coordinates z) onto the unit disk (coordinates w). Integration gives

$$z(w) = A \cdot w \cdot {}_2F_1\left(\frac{1}{N}, \frac{2}{N}; 1 + \frac{1}{N}; w^N\right) + B, \tag{C2}$$

where ${}_pF_q\left(a_1, \ldots, a_p; b_1, \ldots, b_q; \varphi\right)$ denotes the general hypergeometric function. With the constraints $z(0) = 0$ and $z(1) = d$ the center of the N-gon is fixed to the origin and one vertex lies on the real axis at a distance d from the origin. Hence, A and B are obtained as

$$A = \frac{4^{\frac{1}{N}} d\sqrt{\pi}}{\Gamma\left(\frac{1}{2} - \frac{1}{N}\right)\Gamma\left(1 + \frac{1}{N}\right)}, \qquad B = 0, \tag{C3}$$

and the transformed refractive index distribution is given by Eqs. (A2) and (C1) as

$$n'(w) = \left|\frac{(1 - w^N)^{-2/N}}{A}\right|. \tag{C4}$$

Here, it is more difficult to evaluate n' in z coordinates as in Appendix B because an invertible transformation of Eq. (C2) for all N is not at hand. For a square, that is, a regular 4-gon, the route as proposed in the previous subsection can be used, but for a regular hexagon the invertible map of Eq. (C2) must be numerically computed.

APPENDIX D: SCT FROM A RECTANGLE ONTO THE UNIT DISK

It can be shown (the result can be found in Ref. [22]) that the SCT

$$z(w) = \int_0^w \left[\left(\frac{1 - \kappa}{1 + \kappa} - w^2\right)\left(\frac{1 + \kappa}{1 - \kappa} - w^2\right)\right]^{-1/2} dw \tag{D1}$$

maps a rectangle in the z plane onto the unit disk in the w plane. There, κ is defined by $\kappa = \sqrt{1 - k^{-2}}$ as the complementary modulus, where the modulus k itself controls the aspect ratio of the rectangle. The SCT transforms the points $w_{(1,2),(3,4)} = \pm_2\sqrt{(1 \mp_1 \kappa)/(1 \pm_1 \kappa)}$ on the edge of the unit disk onto the four vertices $z_{(1,2),(3,4)} = \pm_2(K \pm_1 iK')$ of the rectangle, where $K = K(k)$ and $K' = K(\sqrt{1 - k^2})$ (the function K again denotes the complete elliptic integral of the first kind). Furthermore $\pm_2$ distinguishes between the two index groups (1, 2) and (3, 4), whereas $\pm_1$ distinguishes between the indices within one of these groups, for example, between 1 and 2 in the first group. Note that the points $w_{(1,2),(3,4)}$ are the four roots in the denominator of the integrand in Eq. (D1). The corresponding points $z_{(1,2),(3,4)}$ can be obtained by evaluating later on the solution of Eq. (D1), Eq. (D3), at $w = w_{(1,2),(3,4)}$. The aspect ratio R_A between the rectangle's height and width is given as a function of k by

$$R_A(k) = \frac{2K'(k)}{2K(k)} = \frac{K(\sqrt{1 - k^2})}{K(k)}. \tag{D2}$$

The integral in Eq. (D1) can be written with the coordinate transformation $\omega = \sqrt{1 - [(1 - w^2)/(1 + w^2)]^2}$ as an elliptic integral of the first kind as

$$z(w) = \int_0^{\omega = \sqrt{1 - \left(\frac{1 - w^2}{1 + w^2}\right)^2}} \frac{d\omega}{\sqrt{1 - k^2\omega^2}\sqrt{1 - \omega^2}}.$$

Hence the SCT, and also after a short calculation its inverse, is given by

$$z(w) = \mathrm{sn}^{-1}\left(\sqrt{1 - \left(\frac{1 - w^2}{1 + w^2}\right)^2}\,\middle|\, k\right), \tag{D3}$$

$$w(z) = \sqrt{\frac{1 - \mathrm{cn}(z|k)}{1 + \mathrm{cn}(z|k)}}, \tag{D4}$$

where Eq. (D3) for the inverse transformation $w(z)$ is in accordance with the result given in exer. 5 on p. 297 in Ref. [22]. The transformed refractive index distribution is given in z coordinates by the modulus of the derivative of Eq. (D3) with respect to z as

$$n'(z) = \left|\frac{dw}{dz}\right| = \left|\frac{\mathrm{dn}(z|k)}{1 + \mathrm{cn}(z|k)}\right|. \tag{D5}$$

Here cn and dn denote two other Jacobi elliptic functions, which are related to sn (see, e.g., Ref. [31]).

[1] J. B. Pendry, D. Schurig, and D. R. Smith, Science **312**, 1780 (2006).

[2] Y. Lai, J. Ng, H. Y. Chen, D. Z. Han, J. J. Xiao, Z. Q. Zhang, and C. T. Chan, Phys. Rev. Lett. **102**, 253902 (2009).

[3] S. A. Cummer, B. I. Popa, D. Schurig, D. R. Smith, and J. Pendry, Phys. Rev. E **74**, 036621 (2006).

[4] D. Schurig, J. J. Mock, B. J. Justice, S. A. Cummer, J. B. Pendry, A. F. Starr, and D. R. Smith, Science **314**, 977 (2006).

[5] D. R. Smith, J. B. Pendry, and M. C. K. Wiltshire, Science **305**, 788 (2004).

[6] M. Yan, Z. Ruan, and M. Qiu, Phys. Rev. Lett. **99**, 233901 (2007).

[7] B. Vasić, G. Isić, R. Gajić, and K. Hingerl, Phys. Rev. B **79**, 085103 (2009).

[8] U. Leonhardt, Science **312**, 1777 (2006).

[9] M. Schmiele, C. Rockstuhl, and F. Lederer, Phys. Rev. A **79**, 053854 (2009).

[10] J. Li and J. B. Pendry, Phys. Rev. Lett. **101**, 203901 (2008).
[11] R. Liu, C. Ji, J. J. Mock, J. Y. Chin, T. J. Cui, and D. R. Smith, Science **323**, 366 (2009).
[12] J. Valentine, J. Li, T. Zentgraf, G. Bartal, and X. Zhang, Nat. Mater. **8**, 568 (2009).
[13] W. X. Jiang, T. J. Cui, H. F. Ma, X. Y. Zhou and Q. Cheng, Appl. Phys. Lett. **92**, 261903 (2008).
[14] W. X. Jiang, T. J. Cui, H. F. Ma, X. M. Yang, and Q. Cheng, Appl. Phys. Lett. **93**, 221906 (2008).
[15] X. Xu, Y. Feng, and T. Jiang, New J. Phys. **10**, 115027 (2008).
[16] M. Rahm, D. A. Roberts, J. B. Pendry, and D. R. Smith, Opt. Express **16**, 11555 (2008).
[17] W. X. Jiang, T. J. Cui, X. Y. Zhou, X. M. Yang and Q. Cheng, Phys. Rev. E **78**, 066607 (2008).
[18] D.-H. Kwon and D. H. Werner, New J. Phys. **10**, 115023 (2008).
[19] N. I. Landy and W. J. Padilla, Opt. Express **17**, 14872 (2009).
[20] M. Rahm, S. A. Cummer, D. Schurig, J. B. Pendry, and D. R. Smith, Phys. Rev. Lett. **100**, 063903 (2008).
[21] W. Yan, M. Yan, and M. Qiu, e-print arXiv:0806.3231v1 [physics.optics].
[22] Zeev Nehari, *Conformal Mapping, International Series in Pure and Applied Mathematics* (McGraw–Hill, New York, 1952), 1st ed.
[23] D. Schurig, J. B. Pendry, and D. R. Smith, Opt. Express **14**, 9794 (2006).
[24] V. S. Varma, Beam Bender and Other Devices in an Isotropic Medium Using Nanocylinders, internship report, Department of Physics at Friedrich Schiller University of Jena, 2009.
[25] C. Rockstuhl, C. Menzel, T. Paul, T. Pertsch, and F. Lederer, Phys. Rev. B **78**, 155102 (2008).
[26] C. Rockstuhl, C. R. Simovski, S. A. Tretyakov, and F. Lederer, Appl. Phys. Lett. **94**, 113110 (2009).
[27] D. Felbacq, G. Tayeb, and D. Maystre, J. Opt. Soc. Am. A **11**, 2526 (1994).
[28] S. Cornbleet, *Microwave and Geometrical Optics* (Academic Press, New York, 1994), 1st ed.
[29] D. Hough, User's Guide to `CONFPACK`, http://www.coventry.ac.uk/ec/~dhough/scpug.zip.
[30] D. E. Marshall and S. Rohde, SIAM J. Numer. Anal. **45**, 2577 (2007).
[31] See, for example, http://mathworld.wolfram.com/JacobiElliptic Functions.html.